Supporting Information

Mixing Thermodynamics and Flory-Huggins Interaction Parameter of Polyethylene Oxide/Polyethylene Oligomeric Blends from Kirkwood-Buff Theory and Molecular Simulations

Fotis Venetsanos, Stefanos D. Anogiannakis, Doros N. Theodorou*

School of Chemical Engineering, National Technical University of Athens, 9 Heroon Polytechniou Street, 15780 Athens, Greece

S1. Forcefield used in the simulations

For the molecular modeling of the PEO/PE oligomeric blends we applied the united-atom version of the Transferable Potentials for Phase Equilibria (TraPPE-UA)[1,2], including a modification introduced by Chen et al.[3]

For non-bonded interactions 12-6 Lennard-Jones and Coulomb potentials are used to model van der Waals and electrostatic interactions, respectively, between different united atoms:

$$U(r_{ij}) = 4\varepsilon_{ij}\left[\left(\frac{\sigma_{ij}}{r_{ij}}\right)^{12} - \left(\frac{\sigma_{ij}}{r_{ij}}\right)^{6}\right] + \frac{q_i q_j}{4\pi\varepsilon_0 r_{ij}} \quad (S1)$$

In order to determine the Lennard-Jones parameters for a pair of dissimilar non-bonded united atoms we use the Lorentz-Berthelot combining rules:

$$\sigma_{ij} = \frac{\sigma_{ii} + \sigma_{jj}}{2} \quad (S2)$$

and

$$\varepsilon_{ij} = \sqrt{\varepsilon_{ii}\varepsilon_{jj}} \quad (S3)$$

Partial charges are placed only on PEO chains and in particular on oxygen atoms and on the CH_x pseudoatoms which are bonded directly to the oxygen atoms. The cutoff radius of the Lennard-Jones potential was set equal to 14 Å for all pairs and analytical tail corrections[4] to the Lennard-Jones interactions were applied based on the assumption of a uniform distribution of pairs beyond the truncation distance. Instead of a standard Ewald summation, we utilized the particle-particle particle-mesh (PPPM) method[5], to calculate the Coulomb interactions in the simulations

involving PEO molecules, significantly reducing the simulation time. Below you may find a table

with the non-bonded parameters used in our simulations.

Table S1. Nonbonded LJ Parameters and Partial Charges

Atom Type	Component	ε (kcal/mol)	σ (Å)	q (e)	References
CH_3	PEO	0.1947	3.75	0.22	[3]
CH_2	PEO	0.0914	3.95	0.22	[3]
O	PEO	0.1292	2.90	-0.44	[3]
CH_3	PE	0.1950	3.75	0.00	[1]
CH_2	PE	0.0910	3.95	0.00	[1]

For the bonded interactions we use: (a) an harmonic bond stretching potential

$$U_{bond}(r) = \frac{k_r}{2}(r - r_0)^2 \quad \text{(S4)}$$

where r is the instantaneous bond length, r_0 is the equilibrium bond length and k_r is the stiffness

of the harmonic potential whose parameter can be found in the table below,

Table S2. Equilibrium Bond Lengths and Force Constants

Bond Type	Component	k_r (kcal/(mol Å²))	r_0 (Å)	References
$CH_3 - O$	PEO	500.00	1.41	[2]
$CH_2 - O$	PEO	500.00	1.41	[2]
$CH_2 - CH_2$	PEO	500.00	1.54	[2]
$CH_3 - CH_2$	PE	500.00	1.54	[1]
$CH_2 - CH_2$	PE	500.00	1.54	[1]

(b) an harmonic angle bending potential

$$U_{bend}(\theta) = \frac{k_\theta}{2}(\theta - \theta_0)^2 \quad (S5)$$

where θ is the instantaneous bond angle, θ_0 is the equilibrium bond angle and k_θ is the stiffness of the potential whose parameter can be found in the table below

Table S3. Equilibrium Bond Angles and Force Constants

Bond Angle Type	Component	k_θ (kcal/(mol deg²))	θ_0 (deg)	References
$CH_2 - O - CH_3$	PEO	60.0135	112.00	[2]
$CH_2 - CH_2 - O$	PEO	49.9780	112.00	[2]
$CH_2 - O - CH_2$	PEO	60.0135	112.00	[2]
$CH_2 - O - CH_3$	PEO	60.0135	112.00	[2]
$CH_2 - CH_2 - CH_3$	PE	62.1000	114.00	[1]
$CH_2 - CH_2 - CH_2$	PE	62.1000	114.00	[1]

And (c) a multi-harmonic dihedral (torsional) angle potential

$$U_{torsion}(\varphi) = \sum_{n=1}^{4} A_n \cos^{n-1}(\varphi) \quad (S6)$$

where φ is the instantaneous dihedral angle, and A_n for $n = 1, 2, 3, 4$ are the coefficients for the cosine series dihedral potential. Note that the *trans* state corresponds to $\varphi = \pi$.

Table S4. Dihedral Angle Potential Parameters.

Dihedral Angle Type	Component	A_1 (kcal/mol)	A_2 (kcal/mol)	A_3 (kcal/mol)	A_4 (kcal/mol)	References
$CH_3 - O - CH_2 - CH_2$	PEO	1.9000	-1.8870	0.6510	4.4370	[2]
$O - CH_2 - CH_2 - O$	PEO	2.0000	-6.0000	1.0000	8.0000	[2]
$CH_2 - O - CH_2 - CH_2$	PEO	1.9000	-1.8870	0.6510	4.4370	[2]
$CH_3 - CH_2 - CH_2 - CH_2$	C12	2.0070	-4.0120	0.2710	6.2900	[1]
$CH_2 - CH_2 - CH_2 - CH_2$	C12	2.0070	-4.0120	0.2710	6.2900	[1]

S2. Excess molar volume, plotted versus the mole fraction of PEO, for PEO/PE oligomeric blends and comparison with corresponding experimental results.
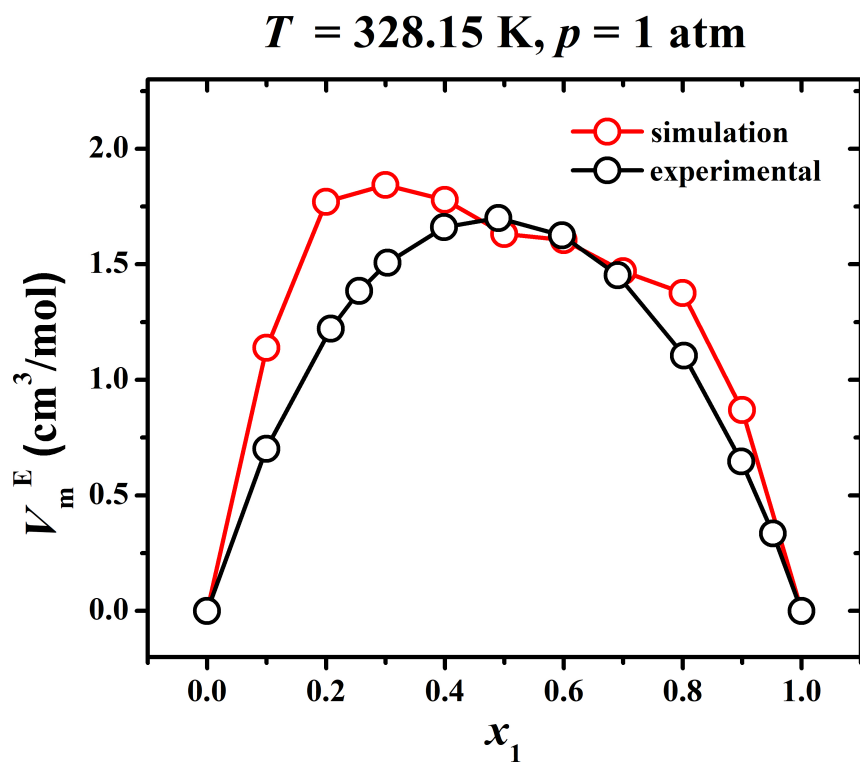
T = 328.15 K, p = 1 atm

Figure S1. Excess molar volume, V_m^E, plotted versus the mole fraction of PEO, x_1, for PEO/PE oligomeric blends as calculated from *NpT* Molecular Dynamics simulations, being compared to experimental data from Rivas et al.[6] at T = 328.15 K, p = 1 atm.

S3. Density plotted versus the mole fraction of PEO, for PEO/PE oligomeric blends and comparison with corresponding experimental results.
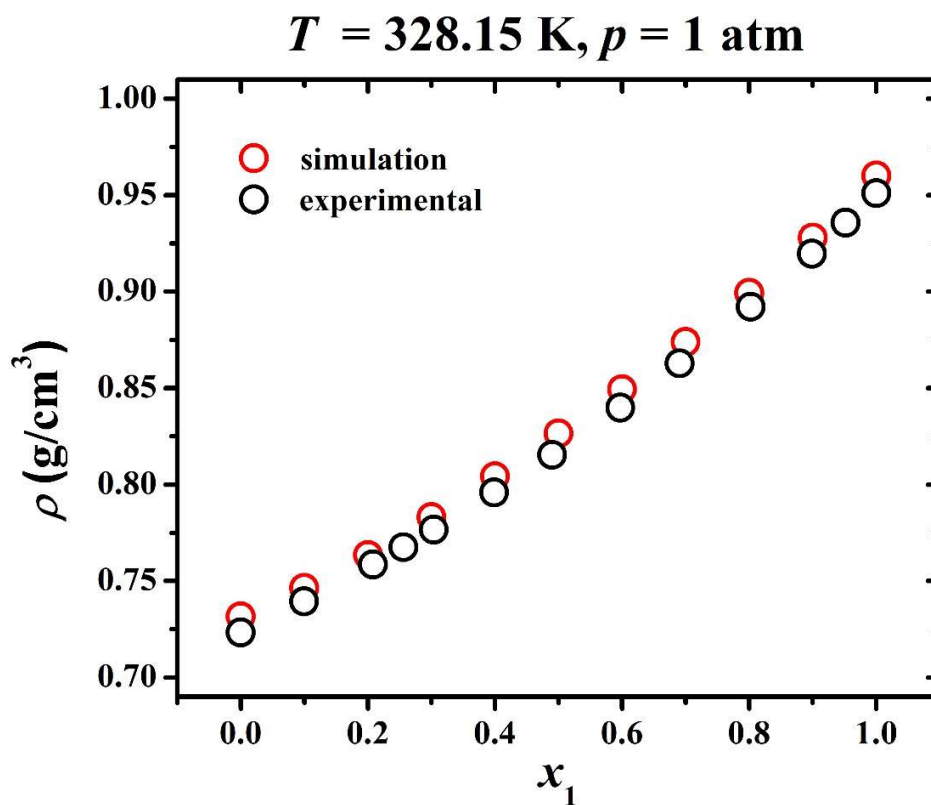
$$T = 328.15 \text{ K}, p = 1 \text{ atm}$$

Figure S2. Density, ρ, plotted versus the mole fraction of PEO, x_1, for PEO/PE oligomeric blends as calculated from NpT Molecular Dynamics simulations, being compared to experimental data from Rivas et al.[6] at $T = 328.15$ K, $p = 1$ atm.

S4. Application of the segment-based method for the estimation of Kirkwood-Buff Integrals in the equimolar PEO/PE blend.
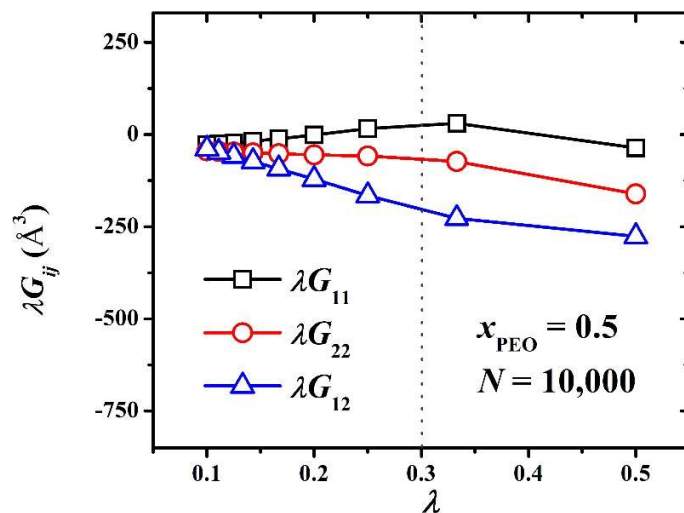

Figure S3. Plot of λG_{11}, λG_{22}, and λG_{12} versus λ for an equimolar PEO/PE binary mixture at $T = 435.26$ K, $p = 1$ atm, for system size of $N = 10,000$ molecules, using the segment-based method. The cutoff value $\lambda = 0.3$ is denoted by the vertical dotted line.

S5. Examples of the polynomial fits to the reduced first derivatives of the chemical

potential, $\dfrac{1}{k_{\mathrm{B}}T}\left(\dfrac{\partial \mu_i}{\partial x_i}\right)_{T,p}$
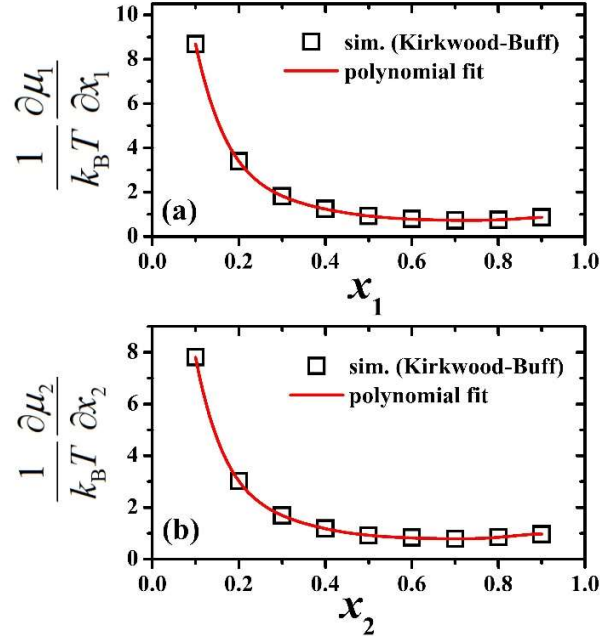

Figure S4. Reduced chemical potential derivatives, $\dfrac{1}{k_{\mathrm{B}}T}\left(\dfrac{\partial \mu_1}{\partial x_1}\right)_{T,p}$ (a) and $\dfrac{1}{k_{\mathrm{B}}T}\left(\dfrac{\partial \mu_2}{\partial x_2}\right)_{T,p}$ (b) plotted

versus the PEO and the PE mole fractions, x_1 and x_2, respectively, for PEO/PE oligomeric blends

at $T = 435.26$ K, $p = 1$ atm.

S6. Molar Gibbs energy of mixing, molar enthalpy of mixing, and molar entropy of mixing, plotted versus the PEO mole fraction, for PEO/PE oligomer binary mixtures and comparison with the corresponding thermodynamic predictions for ideal solutions.
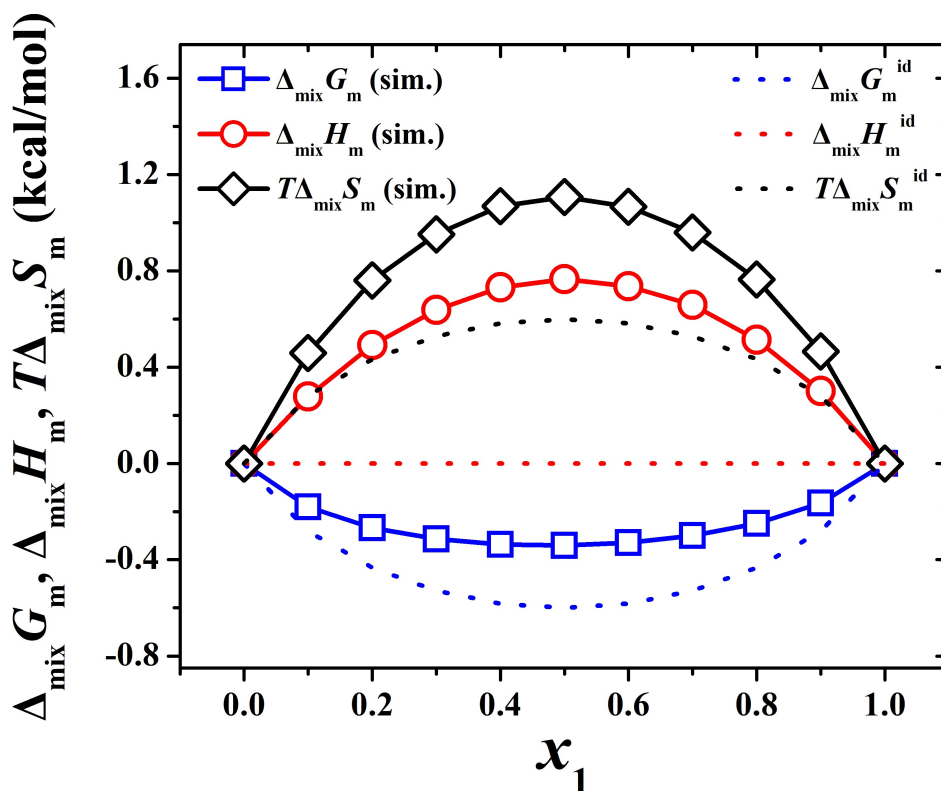

Figure S5. Molar Gibbs energy of mixing, molar enthalpy of mixing, and molar entropy of mixing, plotted versus the PEO mole fraction, x_1, for PEO/PE oligomer binary mixtures at $T = 435.26$ K, $p = 1$ atm. The corresponding ideal molar properties of mixing are shown with dotted lines.

S7. Mean squared radius of gyration

The first structural property we studied is the mean squared radius of gyration, for the PEO and PE chains separately, as a function of the composition. For each chain species, the mean squared radius of gyration R_g^2 is defined by[7]

$$R_g^2 = \frac{1}{N}\left\langle \sum_{k=1}^{N}(\mathbf{r}_k - \mathbf{r}_{cm})^2 \right\rangle \quad (S7)$$

where $\mathbf{r}_k$ is the position of the k-th united atom k, $\mathbf{r}_{cm} = \frac{1}{N}\sum_{k=1}^{N}\mathbf{r}_k$ is the position of the center of mass of the oligomeric chain, N is the number of the united atoms per chain and the average is taken over all chains of the species and all configurations sampled by the simulation.
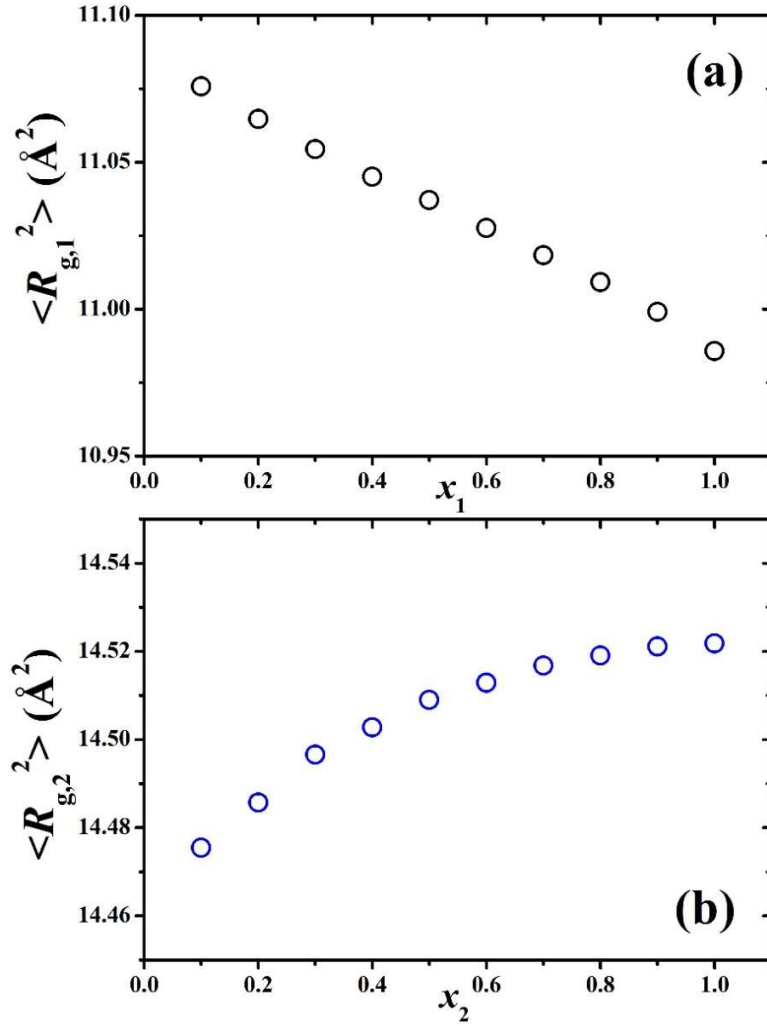
Figure S6. Mean squared radius of gyration, $< R^2_{g,i} >$, plotted versus the mole fraction, x_i, for the blend components PEO, $i = 1$, (a) and PE, $i = 2$, (b).

In Figure S6 (a) and (b) we show our estimates of the mean squared radius of gyration for the PEO and the PE oligomer chains, respectively. We note that the mean squared radius of gyration of the PEO chains increases as x_1 decreases, i.e., moving to blends more dilute in PEO, while the mean squared radius of gyration of the PE chains decreases as x_2 decreases, i.e., moving to blends more dilute in PE. This is a very interesting finding, which indicates an opposite behavior between the two different chains which are mixed, as the initially less stiff PEO chains tend to become stiffer

11

with increasing presence of PE chains, while the initially stiffer PE chains tend to become more coiled (less stiff) with increasing presence of PEO chains. In other words, it seems that different chain species tend to replicate each other's conformational behavior upon mixing. We must also note that the change in mean squared radius of gyration of the PE chains is significantly smaller scale than the one occurring in the PEO chains. Although the chains studied here are too short to extract Flory's characteristic ratio, it has been shown both experimentally[8-10] and from simulations[11-14] that PE chains are much stiffer than PEO chains; the presence of oxygen atoms along the latter's backbone increases the flexibility of the chains. All these findings will be further analyzed and discussed in connection with the dihedral angle distributions.

S8. Dihedral Angle Distributions

In this final subsection, we focus on the probability distribution functions of dihedral angles. The IUPAC convention[15] is adopted here for our dihedral angle representation, φ_{ijkl}, where synperiplanar (*cis*) conformations correspond to $\varphi_{ijkl} = 0^\circ$ while antiperiplanar (*trans*) conformations correspond to $\varphi_{ijkl} = 180^\circ$. The notation φ_{ijkl}, where i, j, k, l are three consecutive united atoms along a chain, denotes the dihedral angle between the plane of united atoms i, j, k and the plane of united atoms j, k, l.

To begin with, in Figure S7 (a) and (b) we observe for the PEO chains that the preferred conformational state for the -C-C-O-C- dihedral angle is the *trans* state at $\varphi = 180^\circ$, while for the -O-C-C-O- dihedral angle it is the *gauche* state at $\varphi = 60^\circ$. While the normalized distributions of the -C-C-O-C- dihedral angle remain practically the same over the various blend compositions, significant changes in conformation are observed in the -O-C-C-O- dihedral angles of the PEO

12

chains. This is the dihedral angle type mainly responsible for the high flexibility of the PEO chains. In particular, as the concentration of PEO chains decreases, more and more *trans* conformations ($\varphi = 180°$) are adopted by -O-C-C-O- torsion angles, leading to more elongated and stiffer PEO chains. This change can be directly linked to our findings showing an increase in the radius of gyration as PEO chain concentration decreases (Figure S6a). We can also identify a direct link to the observed positive deviations from ideal solution behavior: due to the interactions between polar PEO molecules being favorable, the PEO chains tend to unfold in an effort to stay closer to their own species.
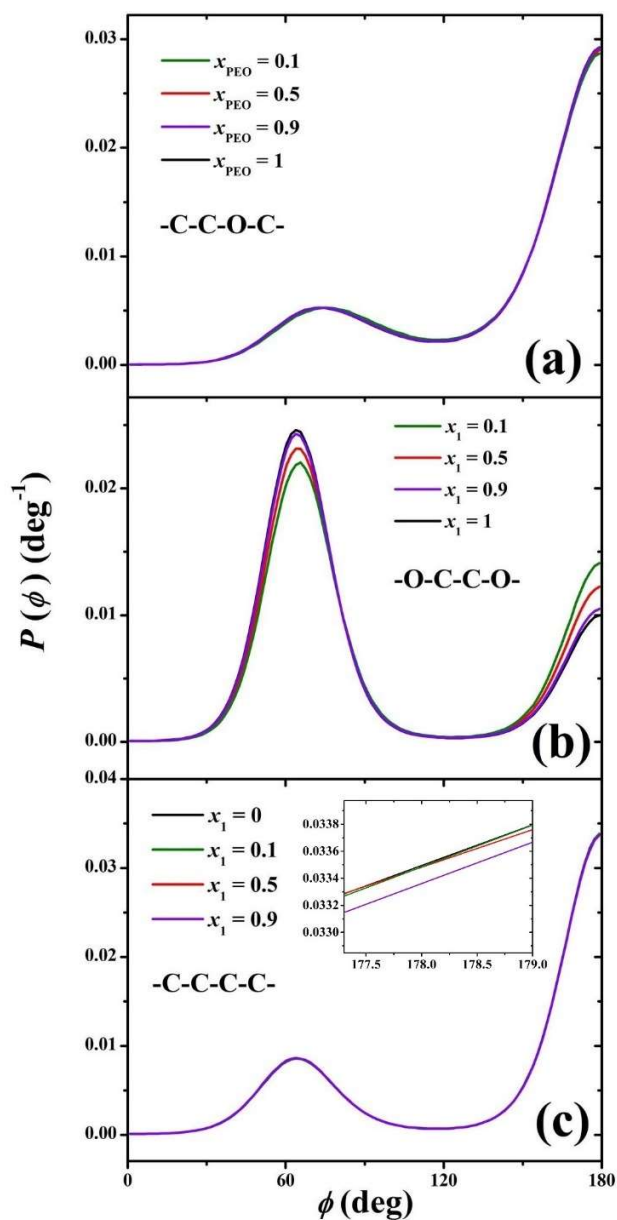
Figure S7. Dihedral angle probability density functions of the -C-C-O-C- angles (a) -O-C-C-O- angles (b) and -C-C-C-C- angles (c), for PEO/PE oligomer binary mixtures with PEO mole fractions $x_1 = 0$, 0.1, 0.5, 0.9, 1 at $T = 435.26$ K, $p = 1$ atm. Inset: enlarged part of figure (c), near the *trans* (180º) state.

On the other hand, for PE chains, there is only one dihedral angle type and its normalized distribution is shown in Figure S7 (c), for various mole fractions. Here the *trans* conformation is much more preferred over the *gauche*. In general, no significant change in the torsion angle distribution is observed for PE across the various mole fractions. However, if we observe the inset of the plot very carefully, we see a slight decrease in the probability of the *trans* state as PE concentration decreases especially for $x_1 = 0.9$. This decrease brings about the small shrinkage we observed in the mean squared PE radius of gyration results of the previous section (Figure S6b), where stiffer PE chains become a bit more coiled upon mixing with PEO chains.

REFERENCES

(1)   Martin, M. G.; Siepmann, J. I. Transferable Potentials for Phase Equilibria. 1. United-Atom Description of n-Alkanes. *J. Phys. Chem.* B **1998**, 102, 2569−2577.

(2)   Stubbs, J. M.; Potoff, J. J.; Siepmann, J. I. Transferable Potentials for Phase Equilibria. 6. United-Atom Description for Ethers, Glycols, Ketones, and Aldehydes. *J. Phys. Chem.* B **2004**, 108, 17596−17605.

(3)   Chen Q. P.; Xie S.; Foudazi R.; Lodge T. P.; Siepmann J. I. Understanding the Molecular Weight Dependence of χ and the Effect of Dispersity on Polymer Blend Phase Diagrams. *Macromolecules*, **2018**, 51, 3774-3787.

(4)   Wood, W. W.; Parker, F. R. Monte Carlo Equation of State of Molecules Interacting with the Lennard-Jones Potential. I. A Supercritical Isotherm at about Twice the Critical Temperature. *J. Chem. Phys.* **1957**, 27, 720−733.

(5)   Hockney R.W.; Eastwood J.W. *Computer Simulation using Particles.* IOP Publishing Ltd. Bristol, England: 1988.

(6)   Rivas, M. A.; Iglesias, T.P.; Pereira, S. N.; Banerji, N. On the permittivity and density measurements of binary systems of {triglyme + (n-nonane or n-dodecane)} at various temperatures. *J. Chem. Thermodyn.* **2005**, 37, 61–71.

(7)   Rubinstein, M.; Colby R.H.; *Polymer Physics*, Oxford: 2003.

(8)   Smith, G. D.; Yoon, D. Y.; Jaffe, R. L.; Colby, R. L.; Krishnamoorti, R.; Fetters, L. J. Conformations and Structures of Poly(oxyethylene) Melts from Molecular Dynamics Simulations and Small-Angle Neutron Scattering Experiments. *Macromolecules* **1996**, 29, 3462−3469.

(9)   Annis, B. K.; Kim, M.-H.; Wignall, G. D.; Borodin, O.; Smith, G. D. A Study of the Influence of LiI on the Chain Conformations of Poly(ethylene oxide) in the Melt by Small-Angle Neutron Scattering and Molecular Dynamics Simulations. *Macromolecules* **2000**, 33, 7544−7548.

(10)   Fetters, L. J.; Lohse, D. J.; Garcia-Franco, C. A.; Brant, P.; Richter, D. Prediction of Melt State Poly(α-olefin) Rheological Properties: The Unsuspected Role of the Average Molecular Weight per Backbone Bond. *Macromolecules* **2002**, 35, 10096−10101.

(11)   Wick, C. D.; Theodorou, D. N. Connectivity-Altering Monte Carlo Simulations of the End Group Effects on Volumetric Properties for Poly(ethylene oxide). *Macromolecules* **2004**, 37, 7026−7033.

(12)   Foteinopoulou, K.; Karayiannis, N. C.; Laso, M.; Krö ger, M. Structure, Dimensions, and Entanglement Statistics of Long Linear Polyethylene Chains. *J. Phys. Chem. B* **2009**, 113, 442−455.

(13)   Logotheti, G. E.; Theodorou, D. N. Segmental and Chain Dynamics of Isotactic Polypropylene Melts. *Macromolecules* **2007**, 40, 2235−2245.

(14)   Tzounis, P. N.; Anogiannakis, S. D.; Theodorou D. N. General Methodology for Estimating the Stiffness of Polymer Chains from Their Chemical Constitution: A Single Unperturbed Chain Monte Carlo Algorithm. *Macromolecules*, **2017**, 50, 4575-4587.

(15)   http://trappe.oit.umn.edu/torsion.html